



Multiperiodic photonic crystals for ultra-sensitive temperature monitoring and polarization switching

Ivan Panyaev, Dmitry Sannikov, Yuliya Dadoenkova, Nataliya Dadoenkova

► To cite this version:

Ivan Panyaev, Dmitry Sannikov, Yuliya Dadoenkova, Nataliya Dadoenkova. Multiperiodic photonic crystals for ultra-sensitive temperature monitoring and polarization switching. *IEEE Sensors Journal*, 2022, 22 (23), pp.22428-22437. <10.1109/JSEN.2022.3217117>. <hal-03854452>

HAL Id: hal-03854452

<https://hal.science/hal-03854452v1>

Submitted on 16 Nov 2022

HAL is a multi-disciplinary open access archive for the deposit and dissemination of scientific research documents, whether they are published or not. The documents may come from teaching and research institutions in France or abroad, or from public or private research centers.

L'archive ouverte pluridisciplinaire **HAL**, est destinée au dépôt et à la diffusion de documents scientifiques de niveau recherche, publiés ou non, émanant des établissements d'enseignement et de recherche français ou étrangers, des laboratoires publics ou privés.



HAL Authorization

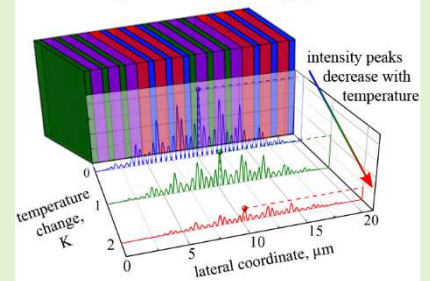
Multiperiodic photonic crystals for ultra-sensitive temperature monitoring and polarization switching

Ivan S. Panyaev, Dmitry G. Sannikov, Yuliya S. Dadoenkova, and Nataliya N. Dadoenkova

Abstract— We study the influence of thermal expansion and thermo-optic effect on optical properties of finite one-dimensional three-periodic photonic crystals of structure $[(ab)^N(cd)^M]^K$ composed of four different nonmagnetic dielectric materials a , b , c , and d . We calculate temperature dependencies and incidence angle dependencies of the transmittivity of TE- and TM-polarized electromagnetic waves, as well as the distribution of energy within these structures. The optimal adjustment of photonic crystal bandgap centers for obtaining the desired transmission characteristics of the temperature-governed photonic bandgap structures is found, and the peculiarities of the energy distributions inside the photonic system are investigated. We propose a sensitive thermal polarization TE|TM switch as well as angular and temperature sensors working at the intraband-mode frequencies exploiting temperature effects.

Index Terms—photonic crystal, photonic bandgap, temperature sensing

1D three-periodic photonic crystal
 $[(ab)^N(cd)^M]^K$
 as a basis of an ultra-sensitive
 temperature monitoring system



I. Introduction

Photonic crystals (PCs) are the optical structures with periodic modulation of the refractive index (or dielectric function). The optical transmittivity and reflectivity of PCs have the photonic band structure consisting in alternating passbands and forbidden bands similar to the electronic band structure of periodic potentials [1–4]. Using various methods, it is possible to shape a given photonic band structure, and thereby effectively control the fundamental optical properties such as reflectivity, group velocity, the rate of spontaneous emission, etc. Thus, many optic effects can be realized in the PCs. For instance, by introducing irregularities or defect layers into regular PCs, one can create defect modes (or inside-bandgap modes). These modes are usually characterized by high and narrow transmission peaks within the bandgaps, whereas the electric field of the light wave is strongly localized inside the defect layer, which in turn leads to many promising applications [5,6]. Indeed, the range of applications of one-dimensional (1D) PCs in photonics and optoelectronic devices today is extremely wide and includes filters, solar cells, fluorescent amplifying devices, sensors, 3D matrices, color displays, etc. [4,7–9].

Recently, attention has been paid to the creation of active photonic devices based on 1D PC with thermally tuned spectra. For example, thermal sensitivity of biosensors implemented on

amorphous $\text{Si}_3\text{N}_4/\text{Si}$ 1D PC is investigated in [10]. A ternary photonic crystal is proposed as a nano-chemical sensor to detect water concentration in ethanol [11]. Temperature-controlled 1D PCs based on mesoporous TiO_2 and SiO_2 layers can serve both as optical filters integrated with organic and inorganic light emitting diodes (OLED and LED) and as low cost IR sensors with low power consumption and manufacturing costs [12]. Multicomponent 1D structures [13] can be used in thermophotovoltaic applications. Temperature dependences of the transmission spectra of hybrid multifunctional superconducting $\text{YBa}_2\text{Cu}_3\text{O}_7$ photonic crystals were studied in Ref. [14]. Using the influence of the thermo-optical and thermal expansion effects in the polymer, a temperature sensor was designed on the base of a ternary PC [15], which operates by measuring the red shift of the transmission peak with an increase of the temperature. Analysis of temperature sensors based on ternary 1D PCs with double defects has been carried out in Ref. [16]. Wide range temperature sensors based on 1D PC with a single defect have been also proposed [17,18].

Such PC structures with a large number of periods (several tens of bilayers) have been successfully fabricated using various methods (e.g. sol-gel, RF-sputtering, etc.) in the recent decades [19–22].

In this paper, we provide a theoretical study of three-periodic

Manuscript received 21 September 2022; accepted 12 October 2022.

This work was supported in part by the Russian Foundation for Basic Research under Grant 19-42-730008, in part by the ministry of Science and Higher Education of the Russian Federation under Grant 075-15-2021-581), in part by École Nationale d'Ingénieurs de Brest, France, and Collège de France under Programme PAUSE. The associate editor coordinating the review of this article and approving it for publication was Prof. Weileun Fang. (Corresponding author: Ivan S. Panyaev.)

I. S. Panyaev, D. G. Sannikov, and N. N. Dadoenkova are with Ulyanovsk State University, 432017 Ulyanovsk, Russia (e-mail: panyaev.ivan@rambler.ru).

Y. S. Dadoenkova is with Lab-STICC (UMR 6285), CNRS, ENIB, 29238 Brest Cedex 3, France (e-mail: dadoenkova@enib.fr), and is also associated with Ulyanovsk State University.

N. N. Dadoenkova is also with Donetsk Institute for Physics and Engineering named after A. A. Galkin, 83114 Donetsk, Ukraine.

Digital Object Identifier 10.1109/JSEN.2022.3217117

1D PCs consisting of four dielectric oxides with different refractive indices. We continue the study begun in Refs. [19–21], where 1D three-periodic PCs with different layer orders are classified according to the magnitude and sign of the optical contrast in the pairs of layers forming the unit cells. The novelty of the type of structures studied here lies in the uniqueness of the layer combination (with a different optical contrast compared to the previously considered structures) which results in a specific behavior of the spectra and flux distribution in the PC. Moreover, in this paper, we take into account the influence of temperature effects on the optical and energy characteristics of such structures. We discuss the possibility of temperature control of the transmission spectra of this type of PC structures using the thermo-optical effect and thermal linear expansion. We also propose a principle of precise polarization-sensitive filters and sensors used in nanophotonics and optoelectronics.

II. GEOMETRY OF 1D THREE-PERIODIC PHOTONIC CRYSTALS

Let us consider finite 1D three-periodic PCs which layers consist of four different dielectrics a , b , c , and d with thicknesses l_a , l_b , l_c , and l_d , respectively. The unit cell of the PC is a combination of two subcells formed by repeating pares of different materials, for example (ab) and (cd) , as shown in Fig. 1. Both the subcells are the finite PCs $(ab)^N$ and $(cd)^M$ with corresponding period lengths $l_1 = l_a + l_b$ and $l_2 = l_c + l_d$. Thus, the structure formula of the PC is $[(ab)^N(cd)^M]^K$, where N and M are the subperiod numbers, and K is the superperiod number. The total length of the PC is $L = K \cdot l_{sup}$, where $l_{sup} = N \cdot l_1 + M \cdot l_2$ is the superperiod length. The structure is surrounded by air.

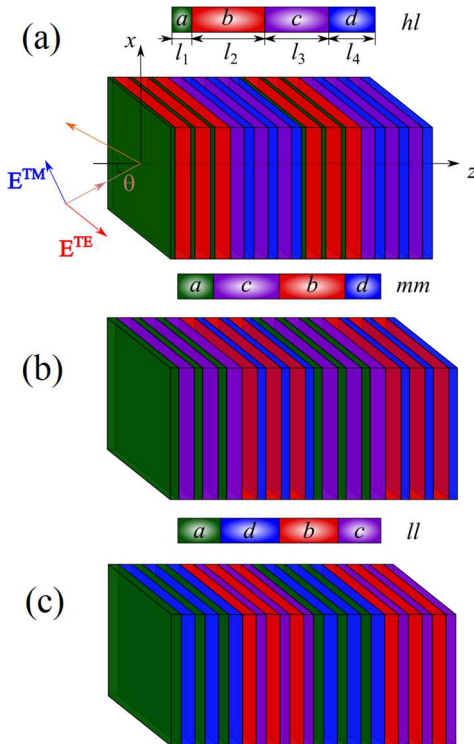


Fig. 1. Schematic of 1D three-periodic PC belonging to the groups (a) **hl** (structure $[(ab)^N(cd)^M]^K$), (b) **mm** (structure $[(ac)^N(bd)^M]^K$), and (c) **ll** (structure $[(ad)^N(bc)^M]^K$), for $N = M = 3$ and $K = 2$. Here E^{TE} and E^{TM} denote electric fields of TE- and TM-polarized electromagnetic waves, and θ is the incidence angle.

An electromagnetic wave of the wavelength λ in vacuum (the angular frequency ω) is incident on the left-hand side surface of the PC under the angle θ , so that the xz is the incidence plane (see Fig. 1).

We choose the layer thicknesses in both subcells to satisfy the Bragg conditions for different Bragg wavelengths λ_{01} and λ_{02} in vacuum:

$$l_{a,b} = \frac{\lambda_{01}}{4n_{a,b}(\lambda_{01})}, \quad l_{c,d} = \frac{\lambda_{02}}{4n_{c,d}(\lambda_{02})} \quad (1)$$

where λ_{01} and λ_{02} correspond to the bandgap centers of the subcells $(ab)^N$ and $(cd)^M$, respectively, constituting the three-periodic PC. Thus, choosing the values $l_{a,b}$ and $l_{c,d}$ in correspondence with Eq. (1), one can modify the position and structure of the bandgap of the hole three-periodic system. As an example, for the constituting materials of the PC we choose the well-known dielectric oxides TiO_2 , SiO_2 , Al_2O_3 and ZrO_2 (further for simplicity denoted as T, S, A, and Z). All these materials are optically isotropic and the normal modes of the considered PC are the electromagnetic waves of TE- and TM-polarizations. The chosen oxides are transparent in the wavelength range (1-5) μm , and the frequency dispersion of their dielectric permittivities are well described by Sellmeier equations [22–25].

The three-periodic four-component PCs can be classified by the absolute values and signs of the dielectric contrasts of materials in the subcells which is defined as dielectric permittivity differences $\Delta\epsilon_{ab} = \epsilon_a - \epsilon_b$ and $\Delta\epsilon_{cd} = \epsilon_c - \epsilon_d$ (see details in Ref. [23]). According to the values of dielectric contrasts, the subcells can be divided into three types: high-contrast subcells with $|\Delta\epsilon| > 3.5$, medium-contrast subcells with $2 < |\Delta\epsilon| < 3.5$, and low-contrast subcells with $|\Delta\epsilon| < 2$, which are denoted as h^\pm , m^\pm and l^\pm (“high”, “medium” and “low”), respectively. Here the upper symbols “ \pm ” are introduced to specify the sign of $\Delta\epsilon$. Thus, the three-periodic PC structures formed by two pairs of different materials can be divided into three groups (**hl**, **mm** and **ll**), where the first and the second characters specify the corresponding pairs, respectively. Each group contains four subgroups, for example, h^+l^+ , h^-l^+ , h^+l^- and h^-l^- for the group **hl**, etc. [23]. The transmittivity spectra of the PCs of the same group demonstrate similarities, and thus the order of the materials forming the sub-cells allows adjusting of the structure in order to have bandgaps with a pre-defined structure.

In addition to topological parameters (Bragg wavelengths defining the thicknesses of the layers) and optical parameters (optical contrast between the pairs of layers forming the PC periods), the spectra of PCs can be also affected by external factors — electric and/or magnetic fields, pressure, temperature, etc. In particular, temperature can have a noticeable effect on the bandgap configuration and on the arrangement of defect modes. Moreover, in the applied aspect, considering the temperature response of the PCs is very important in photonics and quantum electronics, for instance, when creating mirrors for heterostructure laser cavities [20,21,26,27].

In this paper, we assume that the local temperature in all the layers of the PC is the same and is equal to that of the air surrounding it. Temperature manifests itself through two

phenomena: the thermo-optic effect, which affects the refractive index, and the thermal expansion of the layer thicknesses, which modifies the geometry of the system. In what follows, both effects are considered for all the constituents of the system.

Due to the thermo-optic effect, the refractive index of all the constituents of the system undergoes a noticeable variation upon temperature variation. For the considered oxides, this

TABLE I

LINEAR EXPANSION COEFFICIENTS OF THE PC CONSTITUENTS

| Material | Linear thermal expansion coefficient, in 1/K [37] | Maximum expansion of a 100 nm thick film with a temperature change of 100 K, in nm |
|--------------------------------|---|--|
| SiO ₂ | $2 \cdot 10^{-6}$ | 0.02 |
| Al ₂ O ₃ | $8.8 \cdot 10^{-6}$ | 0.09 |
| TiO ₂ | $7.4 \cdot 10^{-6}$ | 0.07 |
| ZrO ₂ | 10^{-5} | 0.1 |

variation is linear with T and is characterized by a constant thermo-optic coefficient γ_j , with:

$$n_j(\Delta t) = n_{0j} + \gamma_j \Delta t, \quad (j = a, b, c, d) \quad (2)$$

where n_{0j} is the refractive index of the medium j at a reference temperature t_0 , which in this study we take as a room temperature (around 293 K).

The values of the thermo-optical coefficients γ_j of the considered oxides vary around $\pm 10^{-3}$ 1/K [28–31] and generally depend on many factors, such as the composition and purity of the material (or presence of impurities), film thickness, temperature range, wavelength and polarization of light, etc. Thus, without loss of generality, we take all the coefficients equal to an average value $\gamma = 10^{-4}$ 1/K.

The variation of the thickness l_j ($j = a, b, c, d$) of the film of material j upon temperature t change is determined by the linear thermal expansion coefficient η_j of that material,

$$l_j = l_{0j} (1 + \eta_j \Delta t) \quad (3)$$

where l_{0j} is a nominal thickness at temperature t_0 for each layer of the system, and $\Delta t = t - t_0$.

Strictly speaking, the linear expansion of films in the transverse direction can lead to deformation or destruction of the structure; therefore, in our calculations, we limited ourselves to an increase in temperature by $\Delta t = 100$ K. Since the lateral dimensions of the layers are much larger than their thickness, we neglect the effect of thermal expansion in the x and y directions. The values of the coefficients of linear thermal expansion are given in Table I. One can estimate that the maximum expansion for the ZrO₂ film, which has the highest coefficient of linear expansion among the materials under study, with a thickness of 100 nm, does not exceed 0.1 nm.

We calculate the transmittivity spectra of the electromagnetic waves of near IR range propagating through the 1D three-periodic PCs using the standard transfer matrix method, see for details, [36]. The material parameters (refractive indices, thermo-optic coefficients, and thermal expansion coefficients) for all the PC constituents were taken in [28–31,33].

III. NUMERICAL ANALYSIS AND DISCUSSION

A. Transmittivity spectra at room temperature

First, we analyze the optical characteristics of tree-periodic PCs at room temperature t_0 and at normal incidence of light ($\theta = 0$, so that the TE- and TM- polarized modes are degenerate).

Figures 2(a)-2(l) show the transmittivity of the PCs from twelve above mentioned subgroups of the three-component structures $[(ab)^N(cd)^M]^K$ as functions of the normalized vacuum Bragg wavelengths $\lambda_{01,02}/\lambda$, with the wavelength of the incident electromagnetic wave $\lambda = 1.55$ μm . We consider the case of $M = N = K = 5$, since these numbers of the cells is sufficient to ensure abrupt boundaries of the bandgaps and pronounced and well distinguishable transmission bands (see our papers [19,20]. The dielectric permittivities of the materials are chosen to be corresponding to the room temperature t_0 [23,24,31,34]. The light and dark areas in Fig. 2 correspond to the transmission bands and the photonic bandgaps, respectively.

From Fig. 2 it follows that the bandgap width is mainly defined by the value of the optical contrast of the subcells forming the three-periodic PC. For instance, for the structures of the group **(hl)** containing the high-contrast and low-contrast subcells, one can see that the bandgaps are broader along the λ_{01}/λ axis, corresponding to the center of the bandgap of the high-contrast subcell **(h)** [see Figs. 2(a), 2(d), 2(g), and 2(j)]. The bandgap along the λ_{02}/λ axis, ensured by low-contrast subcell **(l)**, is less pronounced. In comparison to these spectra, for the structures consisting of two low-contrast subcells **(ll)**, the bandgaps are narrower and not well pronounced along both λ_{01}/λ and λ_{02}/λ axes [see Figs. 2(b), 2(e), 2(h), and 2(k)]. Finally, the structures consisting of medium optical contrast subcells **(mm)** [Figs. 2(c), 2(f), 2(i), 2(l)] possess quite broad bandgaps which are essentially broader than those in the case of **(ll)** groups, but still slightly narrower than those of **(hl)** groups.

However, one can notice some similarities in the spectra of all these structures. In particular, let us consider the central point of each spectrum, where the bandgap centers of both subcells $(ab)^N$ and $(cd)^M$ coincide, being equal to the working wavelength (i. e. $\lambda_{01} = \lambda_{02} = \lambda = 1.55$ μm , or $\lambda_{01,02}/\lambda = 1$). This point corresponds to the bandgap centers for all the considered three-periodic structures from the subgroups with pairs of layers having the identical signs of the optical contrast (**h^+l^+** , **l^+l^+** , and **m^+m^+**). On the contrary, for the PCs from the subgroups with different signs of optical contrast in the pairs of layers (**h^+l^-** , **l^+l^-** , and **m^+m^-**), the bandgaps are either significantly shrank (as for the structures from the subgroups **h^+l^-** and **h^-l^+** in Figs. 2(d) and 2(g)], or they disappear completely giving the space to the transmission bands of the defect modes [structures of the subgroups **l^+l^-** and **l^-l^+** and **m^+m^-** and **m^-m^+** in Figs. 2(e), 2(h) and 2(f), 2(i), respectively].

For further analysis, we choose a three-periodic PC of the subgroup **m^+m^-** , which demonstrates a relatively broad bandgaps with the intraband transmission modes, such as the structure $[(TA)^5(SZ)^5]^5$ (see Fig. 2(i)).

According to (1), in the considered range of λ_{01} and λ_{02} the thicknesses of the layers vary between several tens and several hundred nanometers.

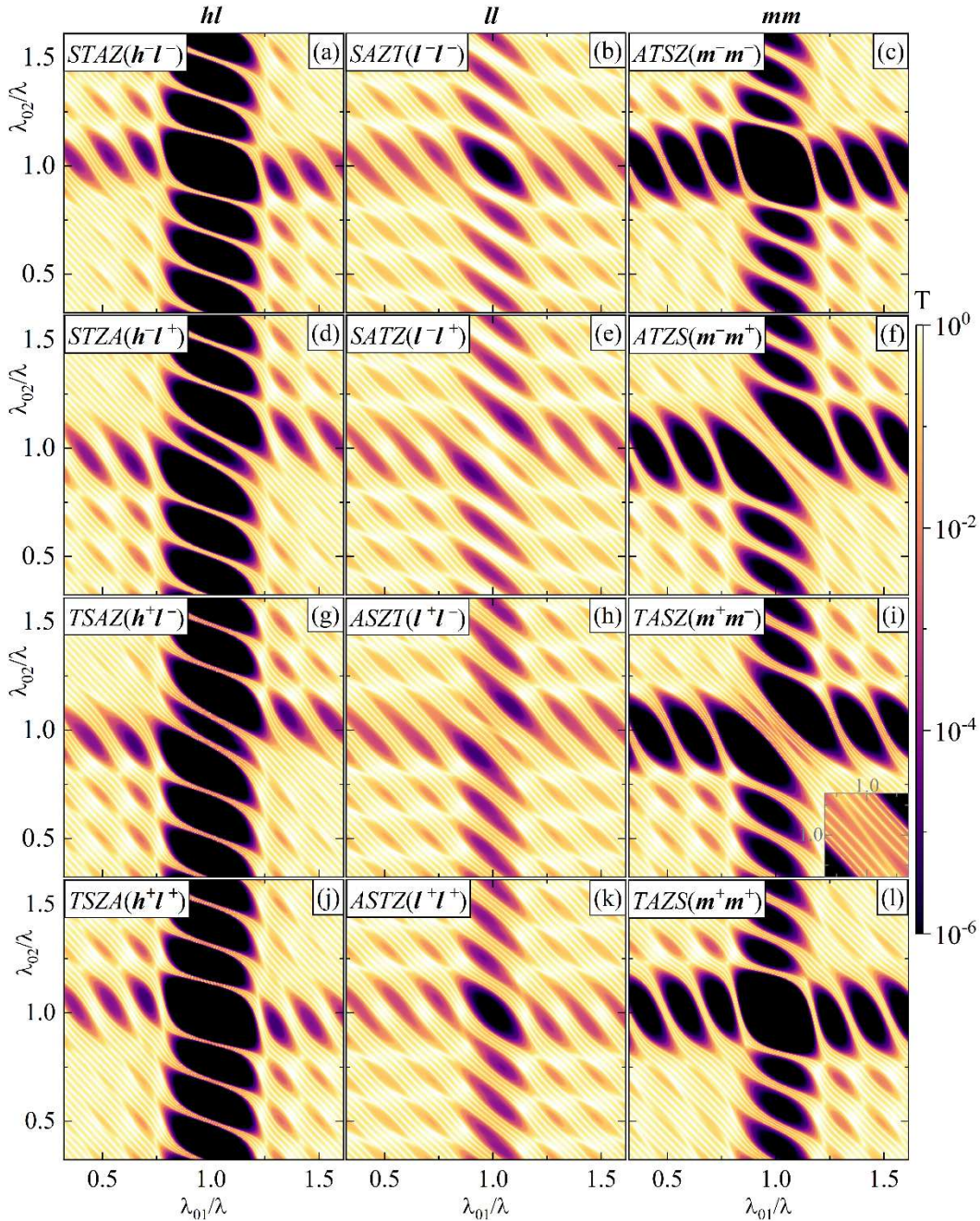


Fig. 2. Transmittivity spectra $T^{TE} = T^{TM}$ (in logarithmic color scale) of three-periodic PCs $[(ab)^5(cd)^5]^5$ for all 12 subgroups (a)-(e) as functions of the reduced vacuum Bragg wavelengths λ_{01}/λ and λ_{02}/λ of the subcells $(ab)^5$ and $(cd)^5$, respectively. The calculations are carried out for the working wavelength $\lambda = 1.55 \mu\text{m}$, for normal incidence ($\theta = 0$), and at room temperature $t_0 = 293 \text{ K}$.

One of the parameters for controlling the spectra of photonic structures is the incidence angle. At oblique incidence, the degeneracy of TE- and TM-modes is canceled, and the spectra of these modes behave differently [23]. In Fig. 3 we show the dependencies of the transmittivity on the reduced vacuum Bragg wavelengths λ_{01}/λ and λ_{02}/λ of the 1st and 2nd subcells of the structure $[(TA)^5(SZ)^5]^5$ for different incidence angles. From Fig. 3, one can see that with an increase in the incidence angle, the bandgaps shift diagonally relatively to the central point $\lambda_{01}/\lambda = \lambda_{02}/\lambda = 1$ towards larger values of λ_{01}/λ and λ_{02}/λ both for TE- and TM-polarized modes. However, the bandgaps of the TE-polarized mode become broader and their edges

become sharper with increase of θ , whereas those of the TM-polarized mode demonstrate narrowing and blurring of the edges.

The key point in the change in the transmission spectra of this structure with an increase in the angle of incidence of light is the alternation of the passbands and the bandgaps for both polarizations (TE and TM) at the point $\lambda_{01}/\lambda = \lambda_{02}/\lambda = 1$. Under normal incidence, this point is located within the transmission band (see Fig. 2(i)). Then, as θ increases, passbands and bandgaps begin to alternate through it. Indeed, at $\theta = 15^\circ$ this point is still in the passband, whereas at $\theta = 30^\circ$ it already corresponds to the bandgap edge (Figs. 3(b), 3(e)), and at

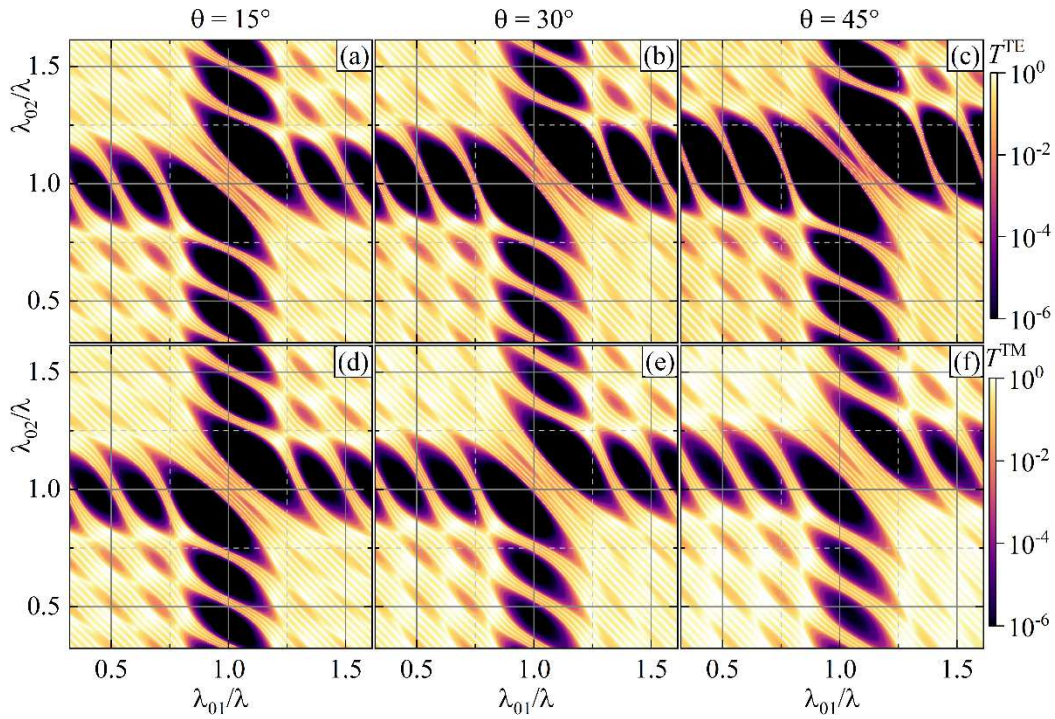


Fig. 3. Transmittivity spectra of the structure $[(\text{TA})^5(\text{SZ})^5]^5$ as functions of the reduced vacuum Bragg wavelengths λ_{01}/λ and λ_{02}/λ of the subcells $(\text{TA})^5$ and $(\text{SZ})^5$, respectively, for different incidence angles $\theta = 15^\circ, 30^\circ$ and 45° . The calculations are carried out for $\lambda = 1.55 \mu\text{m}$ and $t_0 = 293 \text{ K}$. The top panels (a)-(c) and the bottom panels (d)-(f) correspond to TE- and TM-modes, respectively.

$\theta = 45^\circ$, it is inside the bandgap (Figs. 3(c), 3(f)). The practical value of the resulting pattern lies in the possibility of a flexible control of the transmission in the bandgap region by varying the angle of incidence (i. e., photonic bandgap switching).

Further we investigate the influence of temperature variations on the transmittivity spectra in the vicinity of the inside-bandgap modes

B. Temperature tuning of the transmittivity spectra

Let us consider in details the transmittivity of the structure $[(\text{TA})^5(\text{SZ})^5]^5$ at the wavelength interval around the central passband inside the bandgap. Figure 4 shows how the transmittivity spectra at normal incidence $T^{\text{TE}}(\omega, \Delta t) = T^{\text{TM}}(\omega, \Delta t)$ and for the fixed Bragg wavelengths $\lambda_{01} = \lambda_{02} = 1.55 \mu\text{m}$ change with temperature variation $\Delta t = t - t_0 > 0$. It can be interpreted as a temperature-dependent drift of the cross-section of Fig. 2(i) along the line $\lambda_{01}/\lambda = \lambda_{02}/\lambda$. As can be seen from Fig. 4(a), the central transmission peak ($\lambda \approx 1.55 \mu\text{m}$) does not reach unity, but takes a value of about 0.45. The full width at half-maximum (FWHM) of that peak is 3.6 nm (or 2.8 THz-rad). Four high-transmittivity peaks are present on either side of that central one, and they narrow with distance from the central peak. Thus, the number of peaks on either side of the central one is $(K - 1)$. It should be noted that in bi- and three-periodic PCs the number of the subpeaks of the inside-bandgap modes is also equal to $(K - 1)$ [32,35], which is related to the overlapping of the electromagnetic waves localized in the “defect” layers of the structure. In the PC considered here, two inside-bandgap modes merge, and the total number of the peaks in the considered central passband is $(2K - 1)$. The FWHM of the peaks adjacent to the central one

is about 2.4 nm (1.8 THz-rad), whereas the FWHM of the outermost peaks is less than 0.34 nm (250 GHz-rad).

If the layer thicknesses of the structure are initially adjusted to the Bragg wavelengths $\lambda_{01} = \lambda_{02} = 1.55 \mu\text{m}$, the central transmission peak is observed at this wavelength. As the temperature rises, a red shift of the transmission spectrum takes place. Indeed, with an increase of temperature by 100 K, the central peak shifts to a wavelength of 1.56 μm , and its value slightly increases (by approximately 0.02). Thus, the thermal sensitivity of the spectrum of such a three-periodic PC is about 0.1 nm/K, which is 1.6 times more than sensitivity of the defect mode position to the temperature change reported for 1D Si-based PC with a single defect layer [17].

With an increase of the number of supercells, the transmission peaks narrow significantly, as shown in Fig. 4(b) for $K = 10$ without change of the sensitivity to the temperature. Moreover, by choosing the values of λ_{01} and λ_{02} , one can shift the entire spectrum along the wavelength (see Fig. 4(c) for $\lambda_{01} = \lambda_{02} = 1.485 \mu\text{m}$).

Thus, adjusting the geometrical parameters of the three-periodic PC, one can optimize it for monitoring the temperature variations by measuring the shift of a narrow sub-peak of the passband. The temperature sensitivity can be defined as the rate at which a system undergoes a transition from a state of transmission to a state of non-transmission. The latter is a matter of convention: for instance, one can associate a temperature change $[1/\text{K}]$ with the transmittivity decay from $T = 90\%$ to $T = 10\%$ (such transition is widely used, for example, in nonlinear fiber optics to estimate the pulse rise time [40]). For instance, for the structure shown in Fig. 4(c), at $\lambda = 1.55 \mu\text{m}$, the transmittivity changes from 0.9 to 0.1 with the

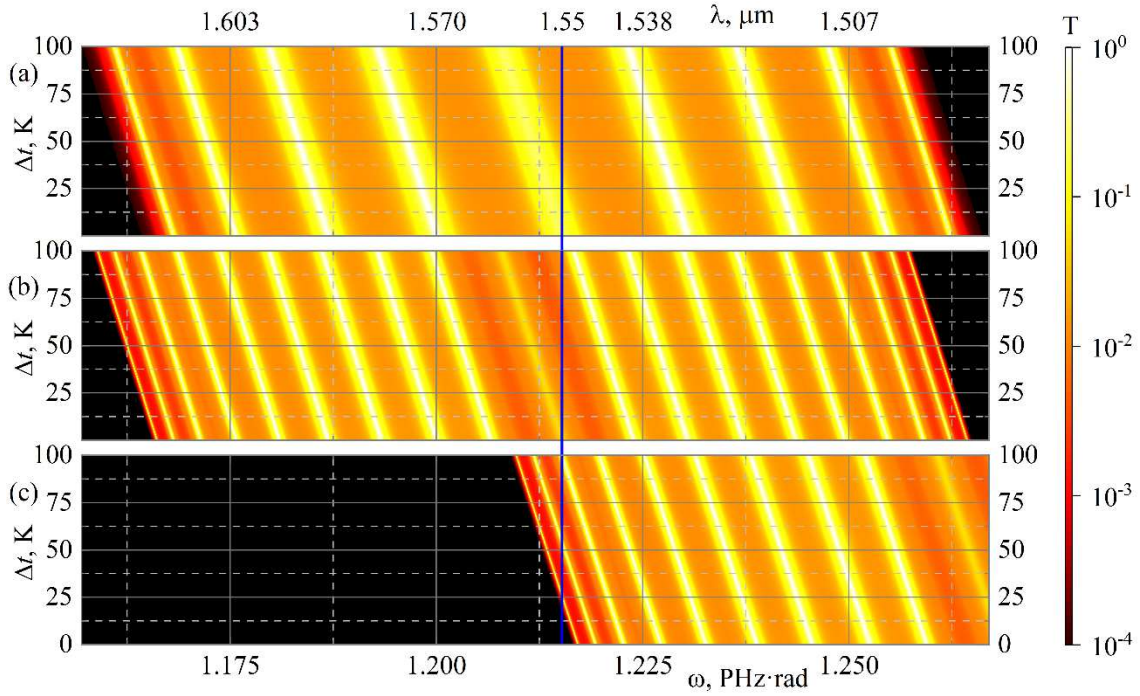


Fig. 4. Transmittivity spectra $T(\omega, \Delta t)$ at normal incidence for the structure: (a) $[(TA)^5(SZ)^5]^5$ with $\lambda_{01} = \lambda_{02} = 1.55 \mu\text{m}$; (b) $[(TA)^5(SZ)^5]^{10}$ with $\lambda_{01} = \lambda_{02} = 1.55 \mu\text{m}$; (c) $[(TA)^5(SZ)^5]^{10}$ with $\lambda_{01} = \lambda_{02} = 1.485 \mu\text{m}$.

temperature drop of 0.45 K (from 25.26 K to 24.81 K). Thus, the temperature sensitivity of a potential sensor, based on the considered structure, can be as high as 2.22 1/K.

As was discussed above, with an increase in the angle of incidence, the degeneracy of the TE and TM polarizations is removed, and the spectra of these modes should be studied separately. Figure 5 shows the dependences of the transmittivity of the structure $[(TA)^5(SZ)^5]^5$ on the angle of incidence θ and temperature variation Δt . At $\Delta t = 0$ and $\theta = 0$, this figure corresponds to the transmittivity at the point $(\lambda_{01}/\lambda, \lambda_{02}/\lambda) = (1, 1)$ on the inset in Fig. 2(i). As can be seen from Fig. 5, at small incidence angles and at relatively small deviations from room temperature t_0 ($\theta < 7^\circ$, $\Delta t < 15$ K), the transmittivity is relatively high for both TE- and TM-modes. At larger θ , however, the difference in the spectra of the TE- and TM-polarized light becomes significant. For instance, at room temperature, the structure does not transmit the TE-polarized light at $\theta > 31^\circ$, which corresponds to the main bandgap. For TM polarization state, a similar picture is observed at the incidence angles interval $34^\circ < \theta < 68^\circ$, and at $\theta > 68^\circ$, one can see the next group of the high-transmittivity passbands.

As the temperature increases, both the passbands and the bandgaps shift towards larger angles of incidence. At a fixed θ , as the deviation from room temperature increases, a transition from one mini-bandgap region to another can occur. For pronounced bands, this transition requires less temperature deviation, as seen in the inset in Fig. 5(a). For example, for a TE-polarized wave in the vicinity of $\theta \approx 29.4^\circ$, initially for $\Delta t \approx 0$, the transmittivity is maximal, $T^{\text{TE}} \sim 1$, then, as the temperature increases, a mini-bandgap is observed with the transmission coefficient of about $10^{-3} - 10^{-1}$, and at $\Delta t > 80$ K,

the passband is again observed. The sensitivity of this transmission bandwidth shift is about $\Delta\theta/\Delta t \approx 0.03^\circ/\text{K}$.

The revealed features of the transmittivity spectra make it possible to achieve a double adjustment of the transmission level of the three-periodic structure: 1) roughly — by changing the incidence angle; 2) smoothly — by varying the temperature. This makes it possible to use these results in sensors with several logical levels of transmission and non-transmission.

C. Temperature tuning of the energy characteristics

Peculiarities of the spectra of three-periodic PCs leads to specific behavior of energy characteristics of these structures, and consideration of the sensitivity of these parameters to temperature changes deserves a separate study.

Figure 6 shows the distributions of the longitudinal component (i. e., along the x -axis) of the Umov-Poynting vector $S_x(\theta, z)$ inside the structure $[(TA)^5(SZ)^5]^5$ for TE- (a) and TM- (b) polarization states of light at room temperature. One can see that $S_x(\theta, z)$ presents beating-like series of maxima at the intervals of the incidence angles corresponding to the high-transmittivity narrow passbands. The intervals of θ where no peaks are observed, correspond to the bandgap of the structure (compare, for instance, Figs. 6(a) and Fig. 5(a) at $\Delta t = 0$). This distribution can be interpreted as a transverse intensity, i. e. the intensity of light at the cross-section of the PC parallel to the z -axis. When considering a PC as a resonator in which standing light waves are observed (with field components $E_y(z)$ for TE- or $H_z(z)$ for TM-polarized waves), one can consider the intensity minima and maxima ($S_x \sim |E_y|^2$ and thus $S_x \sim T^{\text{TE}}$, see [25] for details) as nodes and antinodes, respectively.

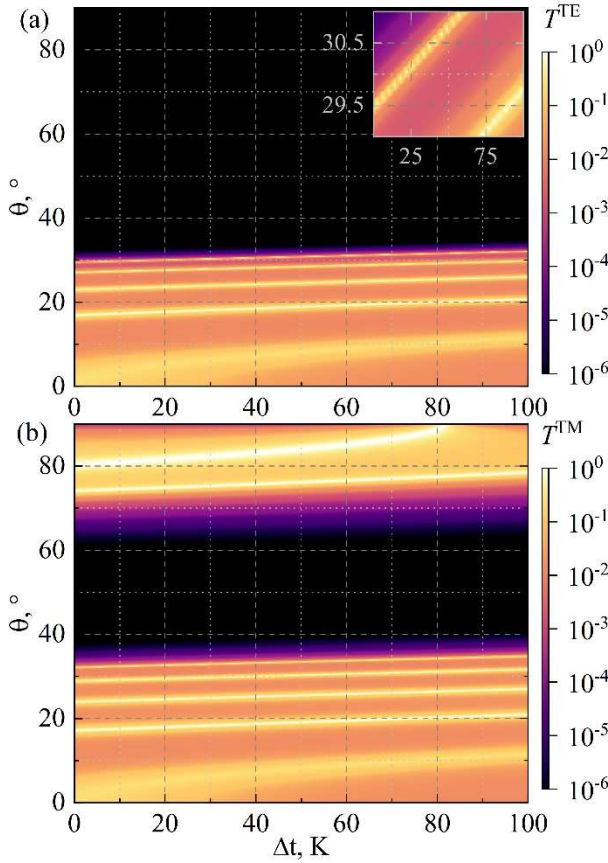


Fig. 5. Evolution of the transmittivity (in logarithmic color scale) of the TE- (a) and TM- (b) modes for the structure $[(TA)^5(SZ)^5]^5$ with the incidence angle θ and temperature variation Δt . Here $\lambda = \lambda_{01} = \lambda_{02} = 1.55$ μm).

Inside the photonic crystal, the antinodes are grouped into “clusters” (in Fig. 6, these clusters are indicated by grey dotted rectangles). The blurring of the antinodes generally decreases when the angle of incidence approaches the bandgap edges for TE- and TM-modes. For TM modes, the antinodes also exist for large angles of incidence, with the maxima merging at grazing incidence. It is interesting to note that the further θ is from the bandgap edge, the less is the number of the peaks inside the “cluster”, whereas the number of the clusters increases.

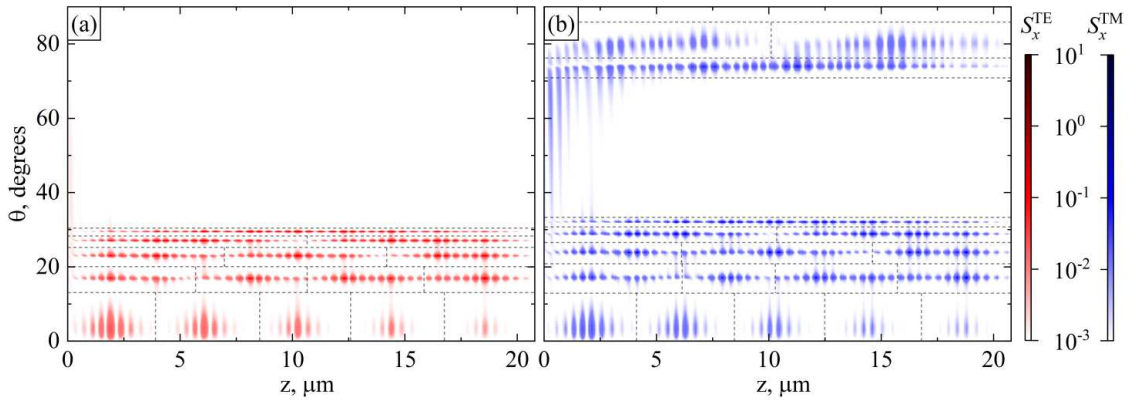


Fig. 6. The longitudinal component of the Umov-Poynting vector $S_x(\theta, z)$ of (a) TE- and (b) TM-polarized light as function of the incidence angle θ and the z -coordinate inside the structure $[(TA)^5(SZ)^5]^5$ at room temperature t_0 .

Figure 7 shows the evolution of the dependences $S_x(\theta, z)$ for two narrow passbands (near $\theta = 28^\circ$ and $\theta = 30^\circ$ for TE-polarization and $\theta = 30^\circ$ and $\theta = 33^\circ$ for TM-polarization states of light) with an increase of temperature. Blue peaks correspond to room temperature t_0 ($\Delta t = 0$), green peaks correspond to $\Delta t = 25$ K, and the red ones to $\Delta t = 50$ K. As can be seen, with increasing temperature by 25 K, the distribution $S_x(\theta, z)$ corresponding to individual transmission bands shifts on average by 0.7° towards larger values of the incidence angle for both TE- and TM-polarizations. The shape of S_x (namely, the number of the peaks and their position along the z -coordinate) is preserved. The angular distance (difference in the angles of incidence) between the transmission peaks for the TE- and TM-modes is more than 1.5° , which is five times greater than that in a ternary (three-component single-periodic) PC [36]. These peculiarities allow us to propose a sensitive thermal polarization TE/TM switch that monitors the temperature variation by measuring the change of the angular distance at which a certain distribution of the transverse component of the Umov-Poynting vector of the corresponding bandwidth is observed.

On the other hand, by fixing the incidence angle, for example, at $\theta = 29.4^\circ$, it is possible to observe the TE-mode at $\Delta t = 0$ K, whereas at $\Delta t = 25$ K, there is no TE-polarized light, but the TM-mode appears, which makes it possible to implement a polarizing TE-TM switch controlled by temperature. Further, for one polarization state, for example, TE, fixing the incidence angle $\theta = 29.4^\circ$ and slightly varying the temperature, one can observe a sharp drop in the intensity $S_x(z)$, which gives a principle of an ultrasensitive thermal sensor. Indeed, an increase in temperature by 1 K leads to a decrease in the peaks of the energy flux by about 2 times (Fig. 8), whereas the spatial position of the peaks does not change. Thus, the relative sensitivity of the longitudinal energy flux to the temperature variations can be estimated as $(S_x|_{\Delta t=0} - S_x|_{\Delta t=1\text{ K}})/(\Delta t S_x|_{\Delta t=0}) = 50\%$ /K. Note that the sensitivity of the temperature sensor can be further increased by increasing the number of subcells (M and N) and superperiods

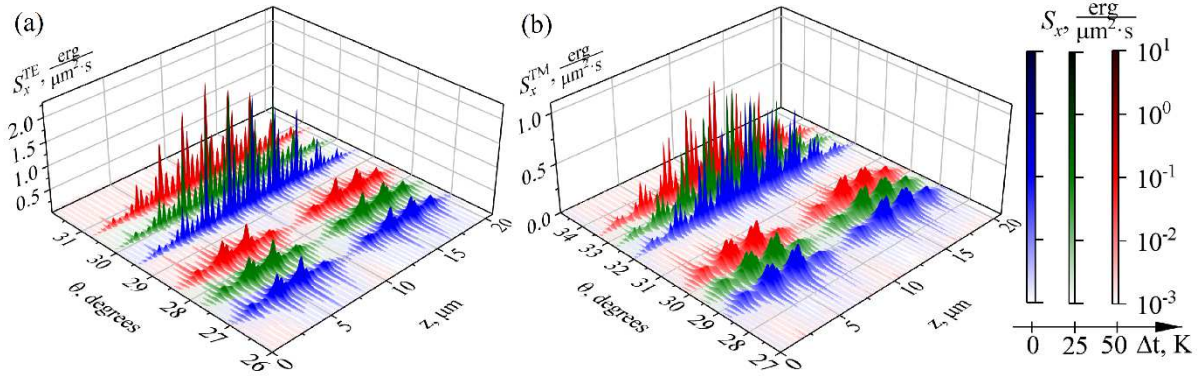


Fig. 7. The longitudinal component of the Umov-Poynting vector $S_x(\theta, z)$ of (a) TE- and (b) TM-polarized light as function of the incidence angle θ and the z -coordinate inside the structure $[(TA)^5(SZ)^5]^5$ for different values of the temperature deviation $\Delta t = 0, 25, 50$ K (blue, green, and red peaks).

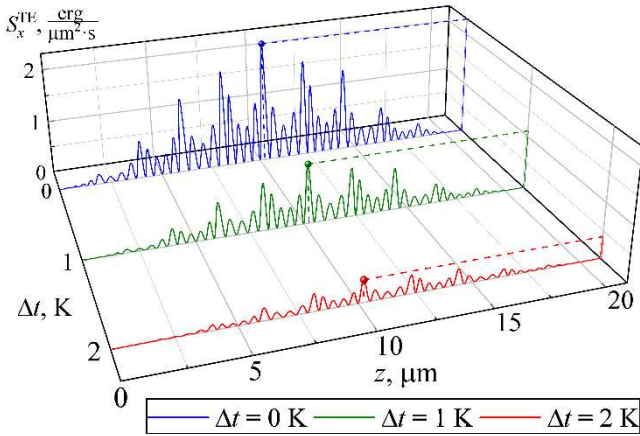


Fig. 8. The longitudinal component of the Umov-Poynting vector $S_x(z)$ of the TE-polarized light as function of the z -coordinate inside the structure $[(TA)^5(SZ)^5]^5$ for different values of the temperature deviation $\Delta t = 0, 1, 2$ K (blue, green, and red curves, respectively) at the incidence angle $\theta = 29.4^\circ$.

(K), which will lead to narrowing of the resonance lines and thus faster decay of the energy flux distribution with small changes of the temperature. The alternation of the transverse intensity bands can also be used in modeling the logic elements of integrated optics, and the ability to work simultaneously in two orthogonal polarizations makes it possible to double the number of potential logic levels/number of states.

IV. CONCLUSION

In this work, we have developed a theoretical analysis of the optical properties of 1D four-component three-periodic photonic crystals $[(ab)^N(cd)^M]^K$ based on TiO_2 , SiO_2 , Al_2O_3 , and ZrO_2 oxides, accounting for the temperature effects on the transmittivity spectra. The considered structures have an advantage over ternary photonic crystals $[(ab)^Nc]^M$, where layers c play a role of regularly repeating defect layers. Four-component three-periodic photonic crystal can be considered as a composite structure in which one of the cells plays the role of a “defect” and the other plays the role of the “regular” photonic crystal.

We focused on the structures with a medium optical contrast in the pairs of layers a, b and c, d of the sub-cells $(ab)^N$ and $(cd)^M$, in contrast to high and low optical contrast studied

previously. Considering thermo-optic effect and effect of temperature expansion, we analyzed the influence of temperature on the transmittivity spectra of TE- and TM-modes and on the intensity distribution inside the photonic crystal. We demonstrate how the choice of the Bragg wavelengths of the subcells can adjust the transmittivity spectra of such a multiperiodic photonic crystal. In addition, the difference in the “resonance” angles of incidence θ corresponding to the transmission peaks of any neighboring modes of TE and TM polarizations can be about 1.5° , which is at least five times as large as in a ternary photonic crystal. This gives a competitive advantage in the development of polarization-sensitive splitters (switcher) or detectors based on multiperiodic photonic crystals.

As the temperature increases, the transmission band shifts at a rate of $\Delta\theta/\Delta t \approx 0.03^\circ/\text{K}$, which provides a double adjustment of the transmission capacity of the structure: by changing the angle of incidence (rough adjustment) and by changing the temperature (smooth adjustment). The sensitivity of the spectrum of three-periodic PC to the variation of temperature is about 0.1 nm/K , which is larger than that of a single-periodic PC with a defect layer. Additionally, such multiperiodic PC can be used for monitoring of tiny deviations of temperature by measuring the intensity distribution along the axis of the structure.

All these peculiarities thus can be useful in the fabrication of sensors that assume the presence of several logical levels of transmission and non-transmission. In addition, the presence of several levels of transmission and non-transmission with different values of the transmittivity makes it possible to use such a structure as an artificial optical synapse for neuromorphic processors, taking into account temperature fluctuations [41]. Adjustable wavelength tuning accuracy can also be useful when working with medical laser sources in the near- and mid-IR ranges.

In view of the foregoing, the type of the structures considered in this paper can be used, in particular, as a basis for creating a thermal sensor integrated into other photonic and/or integrated optics devices, or used as a separate multifunctional photonic device that combines the functions of a thermal sensor (0.1 nm/K or as high as 2.22 1/K for $T = 90^\circ$ to $T = 10^\circ$ transition), an angle sensor (no worse than $0.03^\circ/\text{K}$), a polarization switch and a logic element of an integrated photonics circuit.

REFERENCES

- [1] J. D. Joannopoulos, S. G. Johnson, J. N. J. Winn, and R. D. Meade, *Photonic Crystals. Molding the Flow of Light*, 2nd ed. Princeton: Princeton University Press, 2008.
- [2] R. B. Wehrspohn, H.-S. Kitzerow, and K. Busch, Eds., *Nanophotonic Materials*. Berlin: Wiley-VCH, 2008. doi: 10.1002/9783527621880.
- [3] K. Sakoda, *Optical properties of Photonic Crystals*, 2nd ed. Berlin: Springer, 2005. doi: 10.1017/CBO9781107415324.004.
- [4] Q. Gong and X. Hu, *Photonic Crystals: Principles and Applications*. Pan Stanford, 2014.
- [5] M. L. T. Cossio *et al.*, *Photonic Crystals: Molding the Flow of Light*, 2nd ed., vol. XXXIII, no. 2. 2012. doi: 10.1007/s13398-014-0173-7.2.
- [6] D. W. Prather, A. Sharkawy, S. Shi, J. Murakowski, and G. Schneider, *Photonic crystals : theory, applications, and fabrication*. John Wiley & Sons, 2009.
- [7] H. Shen, Z. Wang, Y. Wu, and B. Yang, "One-dimensional photonic crystals: Fabrication, responsiveness and emerging applications in 3D construction," *RSC Adv.*, vol. 6, no. 6, pp. 4505–4520, 2016, doi: 10.1039/c5ra21373h.
- [8] N. Dadoenkova, Y. Dadoenkova, I. Panyayev, D. Sannikov, and I. Lyubchanskii, "Multiperiodic one-dimensional photonic crystals," in *2D and Quasi-2D Composite and Nanocomposite Materials*, Elsevier, 2020, pp. 103–124. doi: 10.1016/b978-0-12-818819-4.00011-8.
- [9] A. Biswal, R. Kumar, C. Nayak, S. Dhanalakshmi, H. Behera, and I. L. Lyubchanskii, "Analysis of transmission spectra in one-dimensional ternary photonic crystals with complex unit cell," *Optik (Stuttg.)*, vol. 261, p. 169169, Jul. 2022, doi: 10.1016/j.jlleo.2022.169169.
- [10] F. Michelotti and E. Descrovi, "Temperature stability of Bloch surface wave biosensors," *Appl. Phys. Lett.*, vol. 99, no. 23, pp. 2009–2012, 2011, doi: 10.1063/1.3666031.
- [11] S. A. Taya, A. Sharma, N. Doghmosh, and I. Colak, "Detection of water concentration in ethanol solution using a ternary photonic crystal-based sensor," *Mater. Chem. Phys.*, vol. 279, no. June 2021, p. 125772, 2022, doi: 10.1016/j.matchemphys.2022.125772.
- [12] A. T. Exner, I. Pavlichenko, B. V. Lotsch, G. Scarpa, and P. Lugli, "Low-cost thermo-optic imaging sensors: A detection principle based on tunable one-dimensional photonic crystals," *ACS Appl. Mater. Interfaces*, vol. 5, no. 5, pp. 1575–1582, Mar. 2013, doi: 10.1021/am301964y.
- [13] I. Celanovic, F. O'Sullivan, M. Ilak, J. Kassakian, and D. Perreault, "Design and optimization of one-dimensional photonic crystals for thermophotovoltaic applications," *Opt. Lett.*, vol. 29, no. 8, p. 863, 2004, doi: 10.1364/OL.29.000863.
- [14] A. H. Aly, S. E. S. A. Ghany, B. M. Kamal, and D. Vigneswaran, "Theoretical studies of hybrid multifunctional $\text{YBa}_2\text{Cu}_3\text{O}_7$ photonic crystals within visible and infra-red regions," *Ceram. Int.*, vol. 46, no. 1, pp. 365–369, 2020, doi: 10.1016/j.ceramint.2019.08.270.
- [15] D. M. El-Amassi, S. A. Taya, and D. Vigneswaran, "Temperature sensor utilizing a ternary photonic crystal with a polymer layer sandwiched between Si and SiO_2 layers," *J. Theor. Appl. Phys.*, vol. 12, no. 4, pp. 293–298, Dec. 2018, doi: 10.1007/s40094-018-0308-x.
- [16] S. E.-S. A. El-Ghany, "Analysis of Temperature Sensors Based on Ternary One Dimensional Photonic Crystals with Double Defects," *J. Nanoelectron. Optoelectron.*, vol. 14, no. 11, pp. 1532–1538, Oct. 2019, doi: 10.1166/JNO.2019.2653.
- [17] A. Kumar, V. Kumar, B. Suthar, A. Bhargava, K. S. Singh, and S. P. Ojha, "Wide range temperature sensors based on one-dimensional photonic crystal with a single defect," *Int. J. Microw. Sci. Technol.*, pp. 182793–5, 2012, doi: 10.1155/2012/182793.
- [18] O. Soltani, S. Francoeur, and M. Kanzari, "Superconductor-based quaternary photonic crystals for high sensitivity temperature sensing," *Chinese J. Phys.*, vol. 77, pp. 176–188, Jun. 2022, doi: 10.1016/J.CJPH.2022.02.007.
- [19] V. A. Romanova, L. B. Matyushkin, and V. A. Moshnikov, "One-Dimensional Photonic SiO_2 - TiO_2 Crystals: Simulation and Synthesis by Sol-Gel Technology Methods," *Glas. Phys. Chem.*, vol. 44, no. 1, pp. 7–14, 2018, doi: 10.1134/S1087659618010108.
- [20] S. Valligatla *et al.*, "High quality factor 1-D Er^{3+} -activated dielectric microcavity fabricated by RF-sputtering," *Opt. Express*, vol. 20, no. 19, pp. 21214–21222, 2012, doi: 10.1364/OE.20.021214.
- [21] L. González-García, S. Colodrero, H. Míguez, and A. R. González-Elipe, "Single-step fabrication process of 1-D photonic crystals coupled to nanocolumnar TiO_2 layers to improve DSC efficiency," *Opt. Express*, vol. 23, no. 24, p. A1642, 2015, doi: 10.1364/oe.23.0a1642.
- [22] M. Bellingeri, A. Chiasera, I. Kriegl, and F. Scotognella, "Optical properties of periodic, quasi-periodic, and disordered one-dimensional photonic structures," *Opt. Mater. (Amst.)*, vol. 72, pp. 403–421, Oct. 2017, doi: 10.1016/j.optmat.2017.06.033.
- [23] I. S. S. Panyayev, L. R. R. Yafarova, D. G. G. Sannikov, N. N. N. Dadoenkova, Y. S. S. Dadoenkova, and I. L. L. Lyubchanskii, "One-dimensional multiperiodic photonic structures: A new route in photonics (four-component media)," *J. Appl. Phys.*, vol. 126, no. 10, 2019, doi: 10.1063/1.5115829.
- [24] I. S. Panyayev, D. G. Sannikov, N. N. Dadoenkova, and Y. S. Dadoenkova, "Energy flux optimization in 1D multiperiodic four-component photonic crystals," *Opt. Commun.*, vol. 489, p. 126875, Jun. 2021, doi: 10.1016/j.optcom.2021.126875.
- [25] I. S. Panyayev, D. G. Sannikov, N. N. Dadoenkova, and Y. S. Dadoenkova, "Three-periodic 1D photonic crystals for designing the photonic optical devices operating in the infrared regime," *Appl. Opt.*, vol. 60, no. 7, p. 1943, Mar. 2021, doi: 10.1364/ao.415966.
- [26] I. H. Malitson and M. J. Dodge, "Refractive Index and Birefringence of Synthetic Sapphire," *J. Opt. Soc. Am.*, vol. 62, p. 1405, 1972, doi: 10.1364/JOSA.62.001336.
- [27] J. R. Devore, "Refractive indices of rutile and sphalerite," *J. Opt. Soc. Am.*, vol. 41, no. 6, pp. 416–419, 1951, doi: 10.1364/JOSA.41.000416.
- [28] D. L. Wood and K. Nassau, "Refractive index of cubic zirconia stabilized with yttria," *Appl. Opt.*, vol. 21, no. 16, p. 2978, Aug. 1982, doi: 10.1364/AO.21.002978.
- [29] E. D. Palik, Ed., *Handbook of Optical Constants of Solids, volume II*. San Diego: Academic Press, 1998.
- [30] A. A. Liles *et al.*, "Frequency modulated hybrid photonic crystal laser by thermal tuning," *Opt. Express*, vol. 27, no. 8, pp. 11312–11322, Apr. 2019, doi: 10.1364/OE.27.011312.
- [31] A. P. Bakoz *et al.*, "Wavelength stability in a hybrid photonic crystal laser through controlled nonlinear absorptive heating in the reflector," *Light Sci. Appl.*, vol. 7, no. 1, pp. 1–7, Jul. 2018, doi: 10.1038/s41377-018-0043-8.
- [32] R. Ali, M. R. Saleem, P. Pääkkönen, and S. Honkanen, "Thermo-Optical properties of thin-film TiO_2 - Al_2O_3 bilayers fabricated by atomic layer deposition," *Nanomaterials*, vol. 5, no. 2, pp. 792–803, 2015, doi: 10.3390/nano5020792.
- [33] I. Pavlichenko, A. T. Exner, P. Lugli, G. Scarpa, and B. V. Lotsch, "Tunable thermoresponsive $\text{TiO}_2/\text{SiO}_2$ Bragg stacks based on sol-gel fabrication methods," *J. Intell. Mater. Syst. Struct.*, vol. 24, no. 18, pp. 2204–2214, 2013, doi: 10.1177/1045389X12453970.
- [34] G. Gulsen and M. N. Inci, "Thermal optical properties of TiO_2 ," *Opt. Mater. (Amst.)*, vol. 18, pp. 373–381, 2002.
- [35] E. D. Palik, Ed., "Thermo-Optic Coefficients," in *Handbook of Optical Constants of Solids, Vol. 5*, New York: Elsevier, 1997, pp. 115–261. doi: 10.1016/b978-012544415-6.50150-3.
- [36] N. N. N. Dadoenkova, Y. S. Y. S. Dadoenkova, I. S. I. S. Panyayev, D. G. D. G. Sannikov, and I. L. I. L. Lyubchanskii, "One-dimensional dielectric bi-periodic photonic structures based on ternary photonic crystals," *J. Appl. Phys.*, vol. 123, no. 4, 2018, doi: 10.1063/1.5011637.
- [37] V. S. Chirkin, *Thermophysical properties of materials*. Moscow: Fizmatgiz [in Russian], 1959.
- [38] I. H. Malitson, "Interspecimen comparison of the refractive index of fused silica," *J. Opt. Soc. Am.*, vol. 55, no. 10, pp. 1205–1209, 1965, doi: 10.1364/JOSA.55.001205.
- [39] Y. S. Dadoenkova *et al.*, "Confined states in photonic-magnonic crystals with complex unit cell," *J. Appl. Phys.*, vol. 120, no. 7, pp. 73903–9, 2016, doi: 10.1063/1.4961326.
- [40] G. G. P. Agrawal, P. L. Kelley, I. P. Kaminow, and G. G. P. Agrawal, "Nonlinear fiber optics," *Nonlinear Sci. Daw. 21st Century*, p. 467, 2001, doi: 10.1016/B978-0-12-397023-7.00018-8.
- [41] L. F. Abbott and W. G. Regehr, "Synaptic computation," *Nat. 2004 4317010*, vol. 431, no. 7010, pp. 796–803, Oct. 2004, doi: 10.1038/nature03010.

Ivan S. Panyaev was born in Ulyanovsk, Russia, in 1990. He graduated from Ulyanovsk State University, Ulyanovsk, in 2012, majoring in radiophysics and electronics. He received the Ph.D. degree in optics from Ulyanovsk State University in 2017.

From 2015 to 2021, he worked in research positions with the Laboratory of Quantum Electronics and Optoelectronics, Ulyanovsk State University. Currently, he works as a Senior Researcher with the Laboratory of Nonlinear and Microwave Photonics, Technological Research Institute named after S. P. Kapitsa, Ulyanovsk State University. He is the coauthor of one book chapter and more than 30 articles. His research interests are photonic crystals, photonic integrated circuits, fiber laser optics, and nonlinear optics.

Dmitry G. Sannikov was born in 1974. He graduated from Lomonosov Moscow State University, Ulyanovsk Branch [presently, Ulyanovsk State University (UISU)], Ulyanovsk, Russia, in 1996, majoring in solid-state physics. He received the Ph.D. degree in physical and mathematical sciences in 2011.

He currently works as a Docent and a Professor with the Department of Radio Physics and Electronics, UISU, and a Researcher with the Technological Research Institute, UISU. His research interests are integrated optics, photon crystals, optical waveguides, and laser environments.

Yuliya S. Dadoenkova was born in Donetsk, Ukraine, in 1987. She received the master's degree in physics from Donetsk National University, Donetsk, in 2008, the Ph.D. degree in magnetism from the Donetsk Institute for Physics and Engineering, Donetsk, in 2013, and the Habilitation degree to conduct research (HDR) from the University of Western Brittany, Brest, France, in 2022.

She was a contractual Senior Researcher with Yaroslav-the-Wise Novgorod State University, Veliky Novgorod, Russia, from 2015 to 2017, and with the Laboratory of Quantum Electronics and Optoelectronics, Ulyanovsk State University, Ulyanovsk, Russia, from 2014 to 2019. From 2019 to 2021, she was a Postdoctoral Researcher with the École Nationale d'Ingénieurs de Brest (ENIB), Plouzané, France. She is currently a contractual Associate Professor at ENIB and at the CNRS Lab-STICC Laboratory, Brest. She is the coauthor of three book chapters and more than 50 articles. Her research interests include the manipulation of electromagnetic waves in photonic structures based on functional materials, nonspecular effects of electromagnetic and spin-wave beams, and the amplification of surface plasmon polaritons.

Nataliya N. Dadoenkova was born in Donetsk, Ukraine, in 1964. She received the Diploma degree in physics from Donetsk State University, Donetsk, and in 1986 and the Ph.D. degree in theoretical and mathematical physics and the D.Sc. degree from the Donetsk Institute for Physics and Engineering, National Academy of Sciences (NAS) of Ukraine, Donetsk, in 1994 and 2008, respectively.

In 1988, she started her scientific activity at the Donetsk Institute for Physics and Engineering, Academy of Sciences of Ukrainian SSR, Donetsk. From 1994 to 2000 and 2002 to 2014, she worked in the research positions with the Department for Theory of Electronic and Kinetic Properties of Nonlinear Systems, Donetsk Institute for Physics and Technology, NAS of Ukraine. From 2000 to 2002, she was a Postdoctoral Fellow with the Institute of Microstructure Physics of the Max Planck Society, Halle/Salle, Germany. She was a contractual Senior Researcher with the Laboratory of Quantum Electronics and Optoelectronics, Ulyanovsk State University, Ulyanovsk, Russia, from 2014 to 2021. Since 2020, she has been with the Galkin Donetsk Institute for Physics and Engineering, Donetsk, where she works as a Leading Researcher. She is the coauthor of five book chapters and more than 180 scientific publications. Her current research interests include the theory of linear and nonlinear optical effects in uniform and layered magnetic materials, photonic crystals base